

Cite this: *Chem. Sci.*, 2023, 14, 13176

All publication charges for this article have been paid for by the Royal Society of Chemistry

## Bioinformatics-guided discovery of biaryl-linked lasso peptides†

Hamada Saad,<sup>‡\*ab</sup> Thomas Majer,<sup>‡a</sup> Keshab Bhattarai,<sup>‡a</sup> Sarah Lampe,<sup>a</sup> Dinh T. Nguyen,<sup>b</sup> Markus Kramer,<sup>c</sup> Jan Straetener,<sup>d</sup> Heike Brötz-Oesterhelt,<sup>de</sup> Douglas A. Mitchell<sup>b</sup> and Harald Gross<sup>de\*ae</sup>

Lasso peptides are a class of ribosomally synthesized and post-translationally modified peptides (RiPPs) that feature an isopeptide bond and a distinct lariat fold. A growing number of secondary modifications have been described that further decorate lasso peptide scaffolds. Using genome mining, we have discovered a pair of lasso peptide biosynthetic gene clusters (BGCs) that include cytochrome P450 genes. Using mass spectrometry, stable isotope incorporation, and extensive 2D-NMR spectrometry, we report the structural characterization of two unique examples of (C–N) biaryl-linked lasso peptides. Nocapeptin A, from *Nocardia terpenica*, is tailored with a Trp–Tyr crosslink, while longipeptin A, from *Longimycelium tulufanense*, features a Trp–Trp linkage. Besides the unusual bicyclic frame, a Met of longipeptin A undergoes S-methylation to yield a trivalent sulfonium, a heretofore unprecedented RiPP modification. A bioinformatic survey revealed additional lasso peptide BGCs containing P450 enzymes which await future characterization. Lastly, nocapeptin A bioactivity was assessed against a panel of human and bacterial cell lines with modest growth-suppression activity detected towards *Micrococcus luteus*.

Received 9th May 2023

Accepted 27th October 2023

DOI: 10.1039/d3sc02380j

rsc.li/chemical-science

## Introduction

Ribosomally synthesized and post-translationally modified peptides (RiPPs) represent a structurally and functionally diverse group of natural products. Through the combined effects of improved bioinformatic algorithms, genome sequencing campaigns, and isolation/characterization projects, RiPPs feature an extraordinary array of post-translational modifications and architectural scaffolds that cover a broad range of biological functions.<sup>1</sup>

Lasso peptides are one of nearly 50 described classes of RiPPs and display a structurally unique lariat conformation as the class-defining feature. The N-terminus of the core peptide and a side chain carboxylate of an Asp/Glu residing at position

7–9 form a macrolactam ring that is threaded by the C-terminal “tail” residues.<sup>2</sup> Large, steric-locking residues adjacent to the plane of the ring and/or disulfide bridge(s) result in a kinetically trapped rotaxane conformation that endows most lasso peptides with extraordinary thermal and proteolytic stability.<sup>3</sup>

Lasso peptide biosynthesis starts with the ribosomal synthesis of a bipartite precursor peptide (A) that contains N-terminal leader and C-terminal core regions. The leader portion harbors the recognition sequence, which directs the enzymatic processing events *via* interaction with the RiPP precursor recognition element (RRE).<sup>4</sup> Meanwhile, the core region receives all of the post-translational modifications (PTMs).<sup>5</sup> Upon RRE binding, leader peptidolysis is initiated by the co-occurring (B) protein, releasing the core peptide as a substrate for the ATP-dependent lasso cyclase (C).<sup>3a,6</sup> In some lasso peptide biosynthetic pathways, secondary modifications include disulfide bonds, C-terminal methylesterification, N-acetylation, citrullination, O-phosphorylation, glycosylation, epimerization, β-hydroxylation, and aspartimidation.<sup>2b,7</sup> The combination of genome sequencing and enhanced genome-mining algorithms has revealed a large number of RiPP-associated PTMs, including lasso peptides.<sup>7c,8</sup>

Bacteria of the genus *Nocardia* were first studied mainly to understand their pathogenicity. However, metabolic and genomic studies later demonstrated the extraordinary potential of *Nocardia* to produce bioactive and structurally diverse secondary metabolites distinct from other Actinomycetota.<sup>9</sup> In contrast to the well-established and prolific biosynthetic

<sup>a</sup>Department of Pharmaceutical Biology, Institute of Pharmaceutical Sciences, University of Tübingen, Auf der Morgenstelle 8, 72076 Tübingen, Germany. E-mail: hamada.saad@pharm.uni-tuebingen.de; harald.gross@uni-tuebingen.de

<sup>b</sup>Department of Chemistry and the Carl R. Woese Institute for Genomic Biology, University of Illinois at Urbana–Champaign, Urbana, Illinois 61801, USA

<sup>c</sup>Institute of Organic Chemistry, University of Tübingen, Auf der Morgenstelle 18, 72076 Tübingen, Germany

<sup>d</sup>Department of Microbial Bioactive Compounds, Interfaculty Institute of Microbiology and Infection Medicine, University of Tübingen, Auf der Morgenstelle 28, 72076 Tübingen, Germany

<sup>e</sup>Cluster of Excellence: EXC 2124: Controlling Microbes to Fight Infection, University of Tübingen, Tübingen, Germany

† Electronic supplementary information (ESI) available. See DOI: <https://doi.org/10.1039/d3sc02380j>

‡ These authors contributed equally.



potential of *Streptomyces*, only a fraction of the predicted natural products for *Nocardia* have been discovered to date. Known RiPPs from *Nocardia* are currently restricted to the lipolanthines nocavionin,<sup>10a</sup> nocaviogua A and B,<sup>10b</sup> the thiopeptides nocathiacins<sup>10c</sup> and nocardithiocin,<sup>10d</sup> and the chimeric lanthipeptide nocathioamide.<sup>8d</sup>

Based on this promising potential,<sup>8d,9c,11</sup> we mined the genomes of two highly similar *Nocardia terpenica* strains (*i.e.*, IFM 0406 and 0706<sup>T</sup>) for RiPPs using RODEO.<sup>8a</sup> The *Nocardia*-specific bioinformatics analyses identified three putative lasso peptide biosynthetic gene clusters (BGCs) which were not linked to any reported natural product. One *Nocardia* BGC contained a member of protein family PF00067,<sup>12</sup> a predicted cytochrome P450 protein. While P450-encoding genes are relatively rare in bacterial RiPP BGCs,<sup>13</sup> they have yet to be reported in a lasso peptide BGC. Since RiPP-associated P450 proteins perform versatile and complex oxidative transformations,<sup>13,14</sup> we envisioned such BGCs would yield a new type of lasso peptide. Thus, we characterized the products of this pathway, termed the nocapeptins, given the origin was *Nocardia terpenica* (taxonomic order: Corynebacteriales). Bioinformatic expansion outside of *Nocardia* led to the discovery and characterization of the longipeptins, from the phylogenetically distant actinomycete, *Longimycelium tulufanense* (taxonomic order: pseudonocardiales).

## Results and discussion

### Genome mining uncovers lasso peptide BGCs associated with cytochrome P450 enzymes

During an effort to discover new RiPPs from *Nocardia*, we uncovered an unusual lasso peptide BGC (*nop*, Fig. 1). The *nop*

BGC is 5.4 kb in length and consists of six open-reading frames (ORFs), designated *nopA-F*. RODEO was used to examine the constituent gene products,<sup>8a,15</sup> which predicted a class II lasso peptide encoded by *nopA*. Functional annotation of the local ORFs identified the requisite lasso cyclase (NopC, from protein family PF00733), leader peptidase (NopB, PF13471), and discretely encoded RRE domain (NopE, PF05402) (Fig. 1 and Table S1†). As observed for nearly all discrete RRE domains (as opposed to fused cases), the RRE binding to NopA is governed by a characteristic YxxP-containing recognition sequence.<sup>5c,16,24</sup> Furthermore, the BGC includes a putative ABC transporter (NopD, PF00005). Notably, and as the principal criterion for target selection, a cytochrome P450 protein (NopF, PF00067) is locally encoded (Table S1†).

A BLAST-P search of NopB/C followed by RODEO analysis unveiled a small number of similar BGCs (Fig. S2†). One such result was from *Longimycelium tulufanense* CGMCC 4.5737 and was termed *lop* BGC. The *lop* and *nop* BGCs exhibit considerable protein similarity and genetic synteny (Fig. 1 and Table S1†). However, *L. tulufanense* contains two additional genes, *lopG* and *lopH*, encoding a more divergent second cytochrome P450 protein and a protein of unknown function, respectively, suggesting that the resulting lasso peptide will receive additional modifications relative to the *nop* BGC product.

Based on the presence of a canonical Thr(-2), RODEO predicted that leader peptidolysis would occur at Gln/Gly for NopA and LopA, yielding 15-residue core peptides (Fig. 1). Macrocyclization was predicted between Gly1 and Asp8 with Arg14 being the most suitable candidate for a steric-locking residue. The P450 proteins encoded by the *nop/lop* BGCs suggested

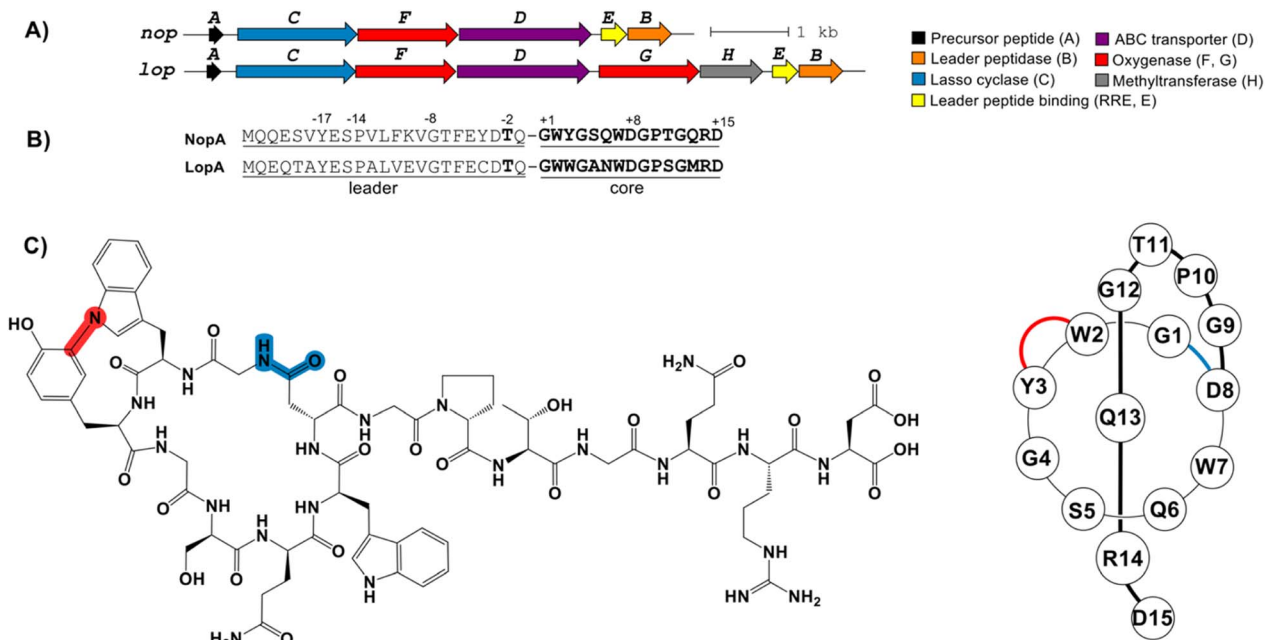


Fig. 1 (A) The *nop* and *lop* BGCs produce nocapeptin A/B and longipeptin A–C, respectively. The A, C, D, E and B genes encode the precursor peptide, lasso cyclase, ABC transporter, RRE, and leader peptidase, respectively. The F and G genes encode two cytochrome P450 proteins while H encodes a hypothetical protein. (B) The leader and core regions of the precursor are indicated. Conserved leader peptide residues are numbered and bolded. (C) The structure formula of the bicyclic lasso peptide nocapeptin A (1, left); schematic drawing of nocapeptin A (1, right).



additional oxidations would be installed; however, bioinformatics cannot predict the specific modification(s) installed by these enzymes. Driven by the new core sequences and the unprecedented inclusion of P450 enzymes in the BGC, we initiated a media screening campaign to isolate and characterize the products of the *nop/lop* BGCs.

### Metabologenomic identification of the lasso peptides

Culture extracts from *N. terpenica* IFM 0406 and *L. tulufanense* using 40 different growth media were screened by LC-MS, with particular attention given to metabolites matching the approximate size of the predicted core peptides ( $m/z$  1500–2000).<sup>17</sup> From the media screen, the MS profiles of IFM 0406 grown in a modified R4 medium at 32 °C exclusively afforded a pair of candidates with  $[M + 2H]^{2+}$  values of 845.3562 (major) and 861.3517 (minor), which were designated as nocapeptin A (1) and nocapeptin B (2), respectively (Fig. S3†). The neutral molecular formula prediction of 1 ( $C_{75}H_{96}N_{22}O_{24}$ ) was consistent with macrolactam formation on the predicted core sequence and loss of 2H, suggesting an oxidative modification within the lasso peptide (Fig. S3†). Relative to 1, the molecular formula of 2 suggested two additional hydroxylation events (Fig. S4†).

The collision-induced dissociation (CID) spectra of 1 and 2 showed a series of y and b ions confirming the NopA sequence (Fig. S4†). Despite the lower probability of observing internal fragments arising from two amide dissociation events, low-intensity y and b fragments were observed that corroborated the amino acid composition of the macrocycle and the residues forming the macrolactam (Tables S2 and S3†). A consistent  $-2.0157$  Da deviation was found in most daughter ions, allowing localization of the secondary modification to the Gly1-Trp2-Tyr3 region.

Using a similar mass-targeted growth media screen,<sup>17</sup> *L. tulufanense* yielded candidate products with  $[M + 2H]^{2+}$  values of 851.3472 (major), 843.3501 (minor), and 844.3395 (trace), designated as longipeptins A–C (3–5), respectively (Fig. S7†). We hypothesized that the post-translational modification statuses of the longipeptides would deviate from 1–2 owing to the presence of *lopG* and *lopH* in the BGC (Fig. 1). Using high-resolution tandem MS (HR-MS/MS), we confirmed the LopA sequence (Fig. S9–S11 and Tables S4–S6†). Besides the anticipated  $-2H$  loss, the neutral molecular formula of longipeptin A (3,  $C_{76}H_{96}N_{22}O_{22}S$ ) was consistent with net addition of oxygen and methylation ( $+CH_2$ ) (Fig. S12 and S13†). While longipeptin B (4) retains methylation, it lacks hydroxylation, suggesting it may be a biosynthetic intermediate. On the other hand, longipeptin C (5) lacks methylation but retains net addition of oxygen (Fig. S12 and S13†).

Despite their structural similarity, the MS<sup>2</sup> spectra of 3 and 4 differed significantly from 5 (Fig. S8†). To explore the discrepancy, and to determine if the net addition of oxygen was from hydroxylation, met oxidation, or another modification, we began with the analysis of the MS<sup>2</sup> spectrum of 5. The resulting y/b ions agreed with the expected core sequence of LopA, a Gly1-Asp8 macrolactam, and loss of 2.0157 Da within the Gly1-Trp2-Trp3 region. Further MS<sup>2</sup> inspection unveiled a new series of  $y_n^*$

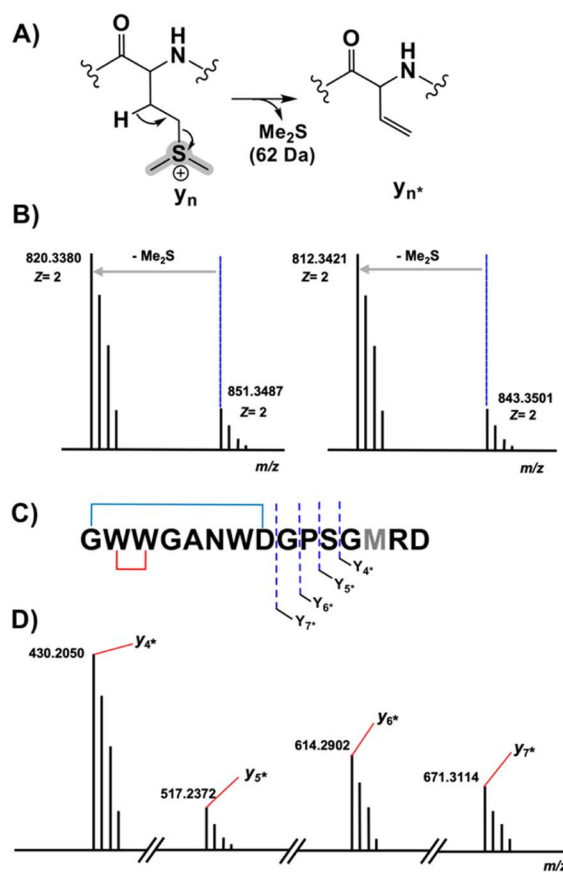


Fig. 2 MS characterization of the longipeptin sulfonium modification. (A) Proposed sulfonium fragmentation resulting in Me<sub>2</sub>S loss. (B) HR-MS/MS data of the  $[M + 2H]^{2+}$  of longipeptin A (left) and longipeptin B (right) exhibiting loss of Me<sub>2</sub>S. (C) Longipeptin core sequence detailing the  $y_n^*$  ions. (D) Annotated MS<sup>2</sup> spectrum of longipeptin  $[M + 2H]^{2+}$  highlighting a new set of y ions ( $y_n - 62 \Rightarrow y_n^*$ ).

( $y_n - 64$  Da) ions consistent with ejection of Me<sub>2</sub>S and thus the presence of Met S-oxide (Fig. 2, S11 and Table S6†). Based on the trace amounts isolated, we conclude that 5 was likely formed by spontaneous air oxidation.

The b ion series of 3 and 4 supported the sequences and location of the previously noted modifications. In 3, the 2H loss and the exclusive hydroxylation were localized by the key b<sub>3</sub> ion. Considering the spectral similarity of 3 and 4 (Fig. S8†) and the annotated b ions, methylation was localized to the Met13-Arg14-Asp15 C-terminal region. Considering several possibilities, S-methylation of Met13 was the most plausible and that such an assignment successfully dereplicated the full MS<sup>2</sup> spectra of 3 and 4. The parent ions of 3 and 4 supported Met13 S-methylation by affording a characteristic M-62 ion, arising from a presumed β-elimination of dimethylsulfide (Fig. 2). In addition, the complete annotation of a new series of y fragments  $y_n^*$ , ( $y_n - 62$ ) including the most intense ions  $y_{4^*-7^*}$ , corroborated the putative modification in 3 and 4 (Fig. S9–S10, Tables S4–S5†).

### Stable isotope labeling of nocapeptin A

To evaluate the chemical nature of the  $-2$  Da mass deviation localized to the first three residues of the nocapeptins (Gly-Trp-



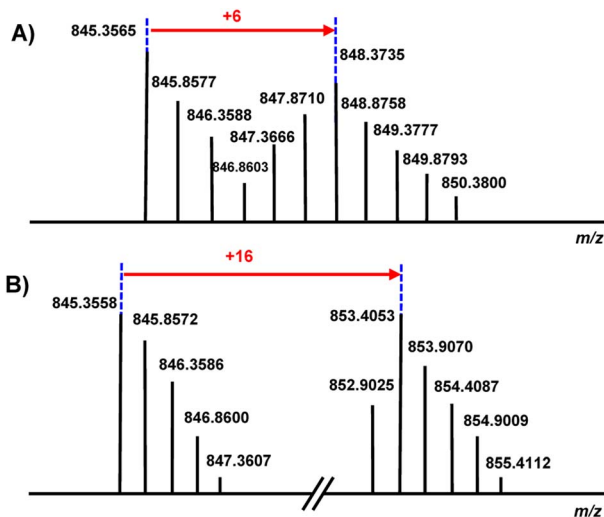


Fig. 3 (A) The MS profile of nocapeptin A (1),  $[M + 2H]^{2+}$  upon culture supplementation with  $[^2H_7]$  L-Tyr. (B) The MS profile of nocapeptin A (1),  $[M + 2H]^{2+}$  upon culture supplementation with  $[^2H_8]$  L-Trp.

Tyr), feeding studies were conducted with  $[^2H_7]$  L-Tyr and  $[^2H_8]$  L-Trp.

For nocapeptin A (1), the LC-MS profiles of IFM 0406 cultures supplemented with  $[^2H_7]$  L-Tyr and  $[^2H_8]$  L-Trp (all C-H protons replaced with deuterium) separately showed incorporation of +6 and +16 Da, respectively (Fig. 3, S5 and S6<sup>†</sup>). The  $[^2H_7]$  L-Tyr feeding data unambiguously demonstrated that the modification was not dehydrogenation, rather a single C-H of Tyr3 was involved in the mass deviation. The  $[^2H_8]$  L-Trp data showed the expected shift for Trp and allowed the conclusion that the C-H bonds of Trp2 and Trp7 were unaltered.

### Structure elucidation of nocapeptin A and longipeptin A

Larger scale cultures of IFM 0406 and *L. tulufanense* under the optimized expression conditions were performed to isolate the material required for structure determination. Subjecting *n*-butanol extracts of the supernatants to reversed phase  $C_{18}$  open

column chromatography and pentafluorophenyl-phase-based HPLC, guided by LC-MS, enabled the isolation of nocapeptin A (1) and traces of longipeptin A (3). The elemental composition of 1 was determined as  $C_{75}H_{96}N_{22}O_{24}$  with 39 ring/double bond equivalents. Extensive NMR analysis was then performed to elucidate the structure of nocapeptin A.  $^1H$ - $^1H$  COSY,  $^1H$ - $^1H$  TOCSY,  $^1H$ - $^{13}C$  HSQC, and  $^1H$ - $^{13}C$  HSQC-TOCSY of the exchangeable NH protons ( $\delta_H$  6.5–9.0) enabled assignment of nearly all spin systems (Fig. 4 and S16–S19<sup>†</sup>). These structural fragments were complemented with  $^1H$ - $^{13}C$  HMBC correlations between their side chain hydrogen and carbon atoms to deliver a complete set of amino acid moieties, 4xGly, 1xSer, 2xGln, 2xAsp, 1xPro, 1xThr and 1xArg (Fig. 4D and S20<sup>†</sup>). Furthermore, three aromatic residues, 2xTrp and 1xTyr, were mainly disclosed with the aid of  $^1H$ - $^{13}C$  HMBC and  $^1H$ - $^1H$  NOESY experiments (Fig. 4D, S28–S29 and S32<sup>†</sup>). In contrast to the typical AA'XX' pattern for Tyr, an alternative ABX/AMX spin system with a characteristic upfield signal ( $\delta_H$  5.46,  $d \approx 2$  Hz)<sup>18</sup> was observed, signifying a *meta* and *para*-disubstituted phenyl substructure. Making use of the  $^1H$ - $^{13}C$  HMBC, and  $^1H$ - $^1H$  NOESY couplings, such a signal was found to be the 2H-Tyr3 (Fig. 4C and S29<sup>†</sup>).

Notably,  $^1H$ -NMR analysis highlighted a discriminative resonance of a single aromatic NH of one Trp residue ( $\delta_H$  10.47, broad singlet), despite two Trp present in the peptide (Fig. S14<sup>†</sup>).  $^1H$ - $^{13}C$  HMBC and  $^1H$ - $^1H$  NOESY correlations assigned the unmodified Trp as Trp7 (Fig. S32<sup>†</sup>), and hence, Trp2 was expected to be modified at the indolic N1 position. The observable couplings obtained from a  $^1H$ - $^{15}N$  HMBC spectrum, between H2-Trp2 and H2-Tyr3 with N1-Trp2 ( $\delta_N$  120.80) in addition to  $^1H$ - $^{13}C$  LR-HSQMBC experiment,<sup>19</sup>  $^1H$ - $^1H$  NOESY relationships, and the isotope labeling experiments permitted the assignment of a biaryl connection between the N1 of Trp2 and C3 of Tyr3 (Fig. 4, S21, S23 and S29<sup>†</sup>). The polypeptide backbone of 1 was assigned *via* the sequential connectivity of the delineated fragments using  $^1H$ - $^{13}C$  HMBC cross-peaks from  $\alpha$ -H resonances to the amide carbonyls of the neighboring amino acid. In addition, the detected  $H_{\alpha,\beta}(i) \rightarrow HN(i+1)$  NOESY

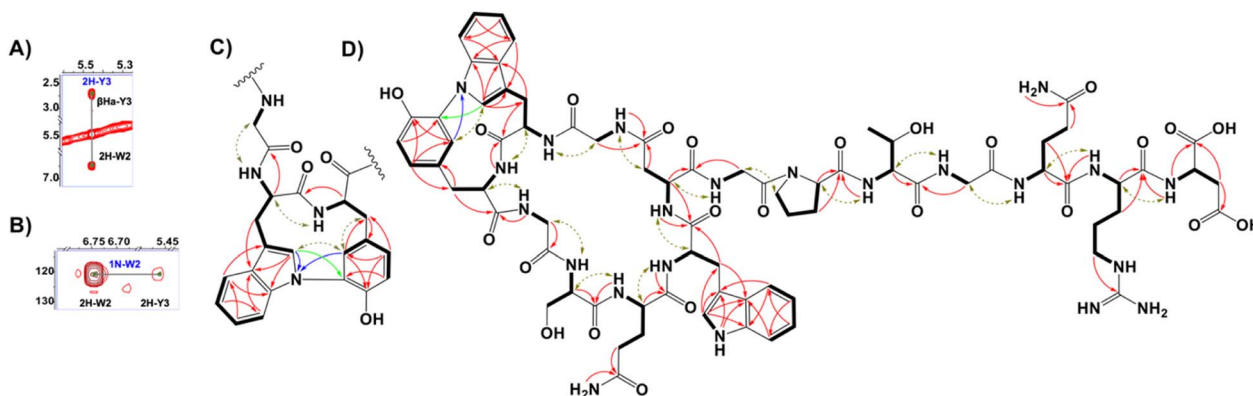


Fig. 4 (A)  $^1H$ - $^1H$  NOESY spectrum highlighting the correlations between 2H-Trp2 and 2H-Tyr3 centers in nocapeptin A (1). (B)  $^1H$ - $^{15}N$  HMBC spectrum showing the correlations between the 1N-Trp2 and 2H-Tyr3 in nocapeptin A (1). (C) The key NMR correlations proving the elucidated biaryl fragment ( $^1H$ - $^1H$  COSY and  $^1H$ - $^1H$  TOCSY: bold lines,  $^1H$ - $^1H$  NOESY: brown arrows,  $^1H$ - $^{13}C$  HMBC: red arrows,  $^1H$ - $^{15}N$  HMBC: blue arrows and  $^1H$ - $^{13}C$  LR-HSQMBC: green arrows). (D) The complete 2D-chemical structure of nocapeptin A (1) with the key NMR correlations.



correlations supported the complete sequence. The macro-lactam between Gly1 and Asp8 was validated similarly (Fig. 4D and S33†). Ultimately, a threaded conformation of **1** was evident with Gln13 and Arg14 assigned as upper and lower plugs, respectively, *via* NOESY correlations (Fig. S23†). The latter experimental findings were in good agreement with the calculated conformation model of the backbone structure, generated with the software LassoHTP.<sup>20</sup>

Using our stable isotope labeling results, we defined the absolute configuration of three amino acids. Thus, the interpretation of the MS-shift patterns showed that both Trp residues and the Tyr unit possess the *L*-configuration. In addition, *L*-Pro10 residue was deduced similarly and the stereochemistry of the remaining chiral residues of **1** were presumed to be *L*-configured. In analogy to other biaryllic RiPPs,<sup>21</sup> we expect that, due to the extra crosslink, atropisomerism is given for nocapeptins. However, since in the <sup>1</sup>H or <sup>13</sup>C NMR spectra neither broad nor doubled resonances were observed, we assume that only one atropisomer is biosynthesized by nature.

Unlike nocapeptin A (**1**), the longipeptin A (**3**) titer was too low for a complete NMR-based structural elucidation. However, keeping in mind the anticipated modification of **3**, the available NMR data permitted partial structural elucidation, including substructures containing the modifications. The annotated spin systems from <sup>1</sup>H-<sup>1</sup>H COSY, <sup>1</sup>H-<sup>1</sup>H TOCSY, and <sup>1</sup>H-<sup>13</sup>C HSQC-TOCSY enabled the assignment of 1xAla, 1xPro, 1xSer, 1xArg, 1xAsn, 2xAsp, and 2xGly (Fig. S45-S47†).

Expectedly, the NMR data showed a significant downfield shift of Met  $\gamma$ -CH<sub>2</sub> ( $\delta_C$  43.13 instead of the typical  $\sim$ 30 ppm). Thus, in agreement with the MS data, we proposed this signal originated from *S*-methylation of Met13, forming a deshielded sulfonium (Fig. 5 and S47†). In addition, three candidate spin systems including the backbone amidic NH,  $\alpha$ -H, and  $\beta$ -H<sub>*a+b*</sub> were assembled in tandem with three aromatic systems to constitute the 3xTrp units (Fig. S47†).

Unfortunately, we could not obtain an adequate <sup>1</sup>H-<sup>1</sup>H NOESY spectrum, which prevented a confident connection of the Trp separate substructures even though weaker allylic <sup>4</sup>J<sub>2H</sub>,  $\beta$ H<sub>*a+b*</sub> couplings, observed in the <sup>1</sup>H-<sup>1</sup>H TOCSY spectrum suggested possible connectivities (Fig. S45 and S47†). The

characteristic indolic NHs of 2xTrp as a pair of singlets ( $\delta_H$  10.18 and 10.55) (Fig. S41A†) and the <sup>1</sup>H-<sup>13</sup>C HMBC correlations identified high-confidence locations of a crosslink and hydroxylation event in the biaryl-containing substructure (Fig. 5, S46 and S47†). Building on the MS data and comparable NMR shifts of **1**, two possible isomers were proposed in which the (N1-C5) biaryl crosslink was adopted alternatively between Trp2 and Trp3 (Fig. 5 and S48†).

### Evaluation of the biological activity and stability of nocapeptin A

Nocapeptin A (**1**) displayed no activity in the National Cancer Institute (NCI) cell-line cytotoxicity screen for antitumor agents. However, when assessed against a panel of bacteria, **1** exhibited growth suppression with an MIC of 16  $\mu$ g mL<sup>-1</sup> towards *Micrococcus luteus* (Tables S9 and 10†). We then tested the stability of **1**, by heating the lasso peptide to 95 °C for 8 h (Fig. S49†) and by carboxypeptidase Y or chymotrypsin treatment (Fig. S50†). Nocapeptin A was unaffected by these procedures, indicating high heat and proteolytic stability.

### Nocapeptins and longipeptins are uniquely tailored bicyclic lasso peptides

The *lop* BGC was expected to encode a lasso peptide with related chemical features. Unusually, longipeptin A (**3**) contained the biaryl linkage of interest in addition to indole hydroxylation and Met *S*-methylation. Despite the low titer, two positional isomers were presented for the (C-N) biaryl fragment (Fig. 5). In analogy to nocapeptins, we assume that N1 of Trp2 is coupled with C5 of Trp3.

Considering their sequence similarity, we predict the P450 proteins NopF/LopF (76% identity, 87% similarity) form the biaryl linkages in **1** and **3**, respectively. Given that Trp hydroxylation is unique to longipeptin, we anticipate LopG, a second P450 protein encoded by the *lop* BGC, performs this reaction. The greater sequence divergence of LopG relative to LopF/NopF (35% and 37% identity, respectively) supports this assignment.

Biaryllic crosslinks are present in several distinct RiPP classes. Crocagin A<sup>22</sup> is a tripeptide RiPP, in which two C-

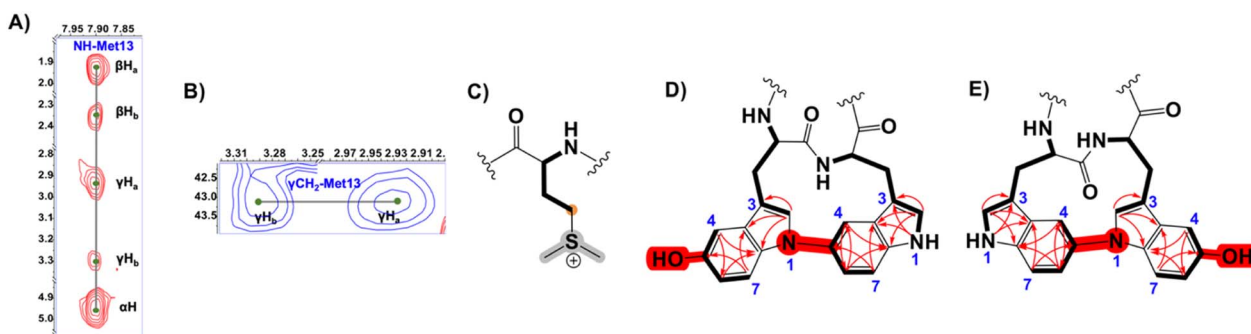


Fig. 5 (A) <sup>1</sup>H-<sup>1</sup>H TOCSY spectrum showing the Met13 spin system of longipeptin A (**3**) (B) <sup>1</sup>H-<sup>13</sup>C HSQC spectrum highlighting the downfield cross-peaks of the  $\gamma$ CH<sub>2</sub> of *S*-methylated Met13 residue in longipeptin A (**3**) (C) Structure of the Met13 sulfonium elucidated by MS/NMR. (D and E) The proposed positional isomers of the (C-N) biaryl fragment of longipeptin A (**3**) with the key NMR couplings (<sup>1</sup>H-<sup>1</sup>H TOCSY, bold lines and <sup>1</sup>H-<sup>13</sup>C HMBC, red arrows) that assembled the constituting structural units, Trp2 and Trp3.



terminal Tyr–Trp residues undergo indole-backbone (C–N) cyclization by a dioxygenase. Atropeptides<sup>21b</sup> represent a P450-modified RiPP class that contains C–C and C–N linkages between Trp and Tyr residues. Biarylittides<sup>23</sup> also contain P450-dependent C–C or C–N linkages between Tyr and His residues. While biarylittides display crosslinks between the first and third residues of the core region, **1** and **3** possess biaryl crosslinks at adjacent aromatic residues.

To shed light on the sequence-function relatedness of NopF/LopF *versus* known P450-modified RiPPs, a sequence similarity network (SSN) was constructed using the top 1000 non-redundant BLAST-P hits of NopF, predicted atropeptide- and biarylittide-associated cytochrome P450 proteins, and 883 P450 proteins encoded within 10 ORFs of an RRE domain.<sup>5c,21b,24</sup> The SSN and similarity/identity analysis (Fig. S51 and S52†) suggested that NopF/LopF are rare examples of P450 proteins within lasso peptide BGCs. A comparative analysis of sequence space also demonstrates that NopF/LopF have significantly diverged from other RiPP-associated cytochrome P450 proteins.

Perhaps the most unusual PTM described in this study is the rare *S*-methylation of Met that affords a trivalent sulfonium. Given the other functional assignments, LopH is the most probable candidate Met *S*-methyltransferase. LopH shares modest sequence similarity (45%) with a hypothetical methyltransferase (WP\_051757134.1, PF00145, Fig. S53†). To support or refute a tentative assignment of LopH as a methyltransferase, we obtained an AlphaFold-predicted structure and used DALI<sup>25</sup> to identify structurally homologous matches from the Protein DataBank.<sup>26</sup> The top hit was a methyltransferase domain-containing subunit of human 5,10-methylenetetrahydrofolate reductase (PDB code: 6fcx). This structure was crystallized with *S*-adenosylhomocysteine (SAH) bound (Fig. S54, S55 and S57†).<sup>27</sup> A comparison of 6fcx and LopH found considerable similarity in the *S*-adenosylmethionine (SAM)-binding sites (specifically, 6fcx residues Glu463, Thr464, Thr481, Ser484, Thr560, and Thr573; which are equivalent to LopH Glu45, Thr46, Thr63, Ser66, Thr126, and Thr134) (Fig. S56 and S58†). As SAM is a common methyl donor for methyltransferases, the predicted structures and the sequence comparison support a tentative assignment of LopH in forming the sulfonium moiety in **3**.<sup>28</sup> Future experimental work will be necessary to confirm this prediction.

Sulfonium groups will readily react with nucleophiles if dealkylation or substitution is possible.<sup>29</sup> The *S*-methylated Met residue of longipeptin A was stable to extraction and purification. The enhanced stability may be attributed to the position of Met within the lasso peptide structure as this position is equivalent to a steric plug residue established in nocapeptin A.

*S*-Methylated RiPPs are quite rare with only two cases of thiopeptides, Sch40832 (ref. 30) and the structurally related thioxamycin<sup>31</sup> and thioactin.<sup>32</sup> *S*-Methylation has also been described for a proteusin that is proposed to contain a single *S*-methylated Cys.<sup>33</sup> Thiol methylation was also illustrated only in a few NRPS cases. Echinomycin and thiocoraline represent NRPS-derived products where *S*-methylation is catalyzed by a SAM-dependent methyltransferase (Ecm18) or a bifunctional enzyme (TioN) with *S*-methyltransferase and amino acid adenylation domains.<sup>34</sup> Maremycin A/B/G and FR900452 provide

further examples of *S*-methylation from BGCs containing homologs of the methyltransferase MarQ.<sup>35</sup>

These examples highlight single *S*-methylation of Cys, thereby differing from the current report on *S*-dimethylmethionine. Unique examples for charged sulfonium units represent bleomycin A2 (ref. 36) and dimethylsulfoniopropionate (DMSP),<sup>37</sup> respectively. Bleomycin A2 carries a 3-aminopropyl-dimethylsulfonium moiety as terminal amine at the Eastern side chain of the molecule. While the freestanding C domain BlmII is postulated to mediate the fusion of the charged side chain with the bleomycin aglycon, the actual biosynthetic origin of 3-aminopropyl-dimethylsulfonium moiety remains enigmatic. DMSPs are well known metabolites found in marine environments. Related compounds have been described, such as gonyol and gonydiol, which are DMSP-derived biosynthetic intermediates of malleicyprols.<sup>37</sup> Generally, DMSP-related metabolites are part of the sulfur cycle, and some marine microorganisms, they protect against osmotic, oxidative, and thermal stresses. In this context, it is notable that the longipeptin producer, *L. tulufanense*, was isolated from a high-salinity lake<sup>38</sup> which may connect the molecular structure of **3** with DMSP ecology.

## Conclusions

In summary, we describe two lasso peptides, **1** and **3**, tailored with four novel PTMs (C–N biaryl linkages between Trp–Trp and Trp–Tyr, *S*-methyl-Met, and 5-hydroxy-Trp), which are installed by a unique combination of RiPP biosynthetic enzymes. The current findings illustrate the value of targeted genome mining in prioritizing novel BGCs from underexplored/rare actinomycetes. As shown earlier, using tandem MS/isotopic incorporation facilitated the gene-to-molecule connection and also compensated for bioinformatic limitations in predicting the chemistry of the secondary PTM enzymes under investigation. Lasso peptides **1** and **3** represent highly tailored entities with 12/13 cyclic C–N biaryl systems fused with an 8-mer macrolactam cycle, respectively.

The BGCs of **1** and **3** encode unique structural features, and the bioinformatic efforts in this study expand the range of PTMs associated with lasso peptide biosynthesis, suggesting that additional oxidative tailoring steps may yet be uncovered (Fig. S59†). To our surprise, the co-occurrence of cytochrome P450 proteins with further maturation enzymes in some retrieved candidate BGCs presents a roadmap to discover additional lasso peptides (Fig. S59†). Given the structural constraint installed by NopF/LopF, future work is warranted to reconstitute the enzymatic activity and substrate scope.<sup>39</sup> Lastly, the prediction that LopH is a founding member of a new Met *S*-methyltransferase family suggests that biochemical characterization of LopH may result in diversifying the existing methylation panel with a sulfonium PTM that can be harnessed in different bioconjugation contexts.<sup>40</sup>

## Data availability

The NMR and MS datasets generated and analysed during the current study are not publicly available but are available from the authors on request.



## Author contributions

H. S. conceptualized the project. H. S., T. M., K. B., S. L., D. T. N., M. K. and J. S. performed experiments. H. S., T. M., S. L., D. T. N., D. A. M. and H. G. analyzed data. H. S. wrote the first draft. H. S., H. B. O., D. A. M. and H. G. edited the paper.

## Conflicts of interest

There are no conflicts to declare.

## Acknowledgements

The NCI-60 anticancer screening service was generously provided by the National Cancer Institute (NCI) as part of the Development Therapeutics Program (DTP). We thank Dr D. Wistuba and her team (Mass Spectrometry Department, Institute for Organic Chemistry, University of Tübingen, Germany) for HR-MS measurements. We thank F. Mier (Pharmaceutical Institute, University of Tübingen) and Z. J. Yang and R. J. Juarez (Dept. of Chemistry, Vanderbilt University, TN, USA) for their help implementing the software LassoHTP. H. S. gratefully acknowledges the Ministry of Higher Education of Egypt (MOHE) for funding. K. B. gratefully acknowledges the funding for a PhD scholarship from the Deutscher Akademischer Austauschdienst (DAAD). D. A. M. acknowledges funding from the U.S. National Institute of General Medical Sciences (GM123998), while H. B.-O. acknowledges funding from the German Center for Infection Research (DZIF, TTU 09-818). Infrastructural support is from the Cluster of Excellence EXC 2124 (project ID 390838134) funded by the Deutsche Forschungsgemeinschaft (DFG).

## Notes and references

- (a) M. Montalbán-López, T. A. Scott, S. Ramesh, I. R. Rahman, A. J. van Heel, J. H. Viel, V. Bandarian, E. Dittmann, O. Genilloud, Y. Goto, M. J. Grande Burgos, C. Hill, S. Kim, J. Koehnke, J. A. Latham, A. J. Link, B. Martinez, S. K. Nair, Y. Nicolet, S. Rebuffat, H.-G. Sahl, D. Sareen, E. W. Schmidt, L. Schmitt, K. Severinov, R. D. Süßmuth, A. W. Truman, H. Wang, J.-K. Weng, G. P. van Wezel, Q. Zhang, J. Zhong, J. Piel, D. A. Mitchell, O. P. Kuipers and W. A. van der Donk, *Nat. Prod. Rep.*, 2021, **38**, 130–239; (b) Y. Li and S. Rebuffat, *J. Biol. Chem.*, 2020, **295**, 34–54; (c) C. Ongpipattanakul, E. K. Desormeaux, A. DiCaprio, W. van der Donk, D. A. Mitchell and S. K. Nair, *Chem. Rev.*, 2022, **122**, 14722–14814.
- (a) M. O. Maksimov, S. J. Pan and A. J. Link, *Nat. Prod. Rep.*, 2012, **29**, 996–1006; (b) J. D. Hegemann, K. J. Dit-Foque and X. Xie, in *Comprehensive Natural Products III: Chemistry and Biology*, ed. H.-W. Liu and T. P. Begley, Elsevier, 3rd edn, 2020, vol. 2, pp. 206–228.
- (a) J. D. Hegemann, M. Zimmermann, X. Xie and M. A. Marahiel, *Acc. Chem. Res.*, 2015, **48**, 1909–1919; (b) J. D. Hegemann, in *Methods in Enzymology*, ed. L. M. Hicks, Elsevier, 2021, vol. 663, pp. 177–204; (c) J. D. Hegemann, *ChemBioChem*, 2020, **21**, 7–18.
- (a) S. Zhu, C. D. Fage, J. D. Hegemann, A. Mielcarek, D. Yan, U. Linne and M. A. Marahiel, *Sci. Rep.*, 2016, **6**, 35604; (b) T. Sumida, S. Dubiley, B. Wilcox, K. Severinov and S. Tagami, *ACS Chem. Biol.*, 2019, **14**, 1619–1627; (c) A. Alfi, A. Popov, A. Kumar, K. Y. J. Zhang, S. Dubiley, K. Severinov and S. Tagami, *ACS Synth. Biol.*, 2022, **11**(6), 2022–2028; (d) A. M. Kretsch, M. G. Gadgil, A. J. DiCaprio, S. E. Barrett, B. L. Kille, Y. Si, L. Zhu and D. A. Mitchell, *Biochem*, 2023, **62**, 956–967.
- (a) B. J. Burkhart, G. A. Hudson, K. L. Dunbar and D. A. Mitchell, *Nat. Chem. Biol.*, 2015, **11**, 564–570; (b) J. Koehnke, G. Mann, A. F. Bent, H. Ludewig, S. Shirran, C. Botting, T. Lebl, W. E. Houssen, M. Jaspars and J. H. Naismith, *Nat. Chem. Biol.*, 2015, **11**, 558–563; (c) A. M. Kloosterman, K. E. Shelton, G. P. van Wezel, M. H. Medema and D. A. Mitchell, *mSystems*, 2020, **5**, e00267.
- (a) K. P. Yan, Y. Li, S. Zirah, C. Goulard, T. A. Knappe, M. A. Marahiel and S. Rebuffat, *ChemBioChem*, 2012, **13**, 1046–1052; (b) A. J. DiCaprio, A. Firouzbakht, G. A. Hudson and D. A. Mitchell, *J. Am. Chem. Soc.*, 2019, **141**, 290–297; (c) J. D. Koos and A. J. Link, *J. Am. Chem. Soc.*, 2019, **141**, 928–935.
- (a) C. Zhang and M. R. Seyedsayamdost, *ACS Chem. Biol.*, 2020, **15**, 890–894; (b) L. Cao, M. Beiser, J. D. Koos, M. Orlova, H. E. Elashal, H. V. Schröder and A. J. Link, *J. Am. Chem. Soc.*, 2021, **143**, 11690–11702; (c) L. A. Harris, P. M. B. Saint-Vincent, X. Guo, G. A. Hudson, A. J. DiCaprio, L. Zhu and D. A. Mitchell, *ACS Chem. Biol.*, 2020, **15**, 3167–3175.
- (a) J. I. Tietz, C. J. Schwalen, P. S. Patel, T. Maxson, P. M. Blair, H.-C. Tai, U. I. Zakai and D. A. Mitchell, *Nat. Chem. Biol.*, 2017, **13**, 470–478; (b) W. L. Cheung-Lee and A. J. Link, *J. Ind. Microbiol. Biotechnol.*, 2019, **46**, 1371–1379; (c) D. Y. Travin, D. Bikmetov and K. Severinov, *Front. Genet.*, 2020, **11**, 26; (d) H. Saad, S. Aziz, M. Gehringer, M. Kramer, J. Straetener, A. Berscheid, H. Brötz-Oesterhelt and H. Gross, *Angew. Chem., Int. Ed.*, 2021, **60**, 16472–16479.
- (a) D. Männle, S. M. K. McKinnie, S. S. Mantri, K. Steinke, Z. Lu, B. S. Moore, N. Ziemert and L. Kaysser, *mSystems*, 2020, **5**, e00125; (b) D. Dhakal, V. Rayamajhi, R. Mishra and J. K. Sohng, *J. Ind. Microbiol. Biotechnol.*, 2019, **46**, 385–407; (c) A. Engelbrecht, H. Saad, H. Gross and L. Kaysser, *Microb. Physiol.*, 2021, **31**, 217–232; (d) Q. Luo, S. Hiessl and A. Steinbüchel, *Environ. Microbiol.*, 2014, **16**, 29–48.
- (a) V. Wiebach, A. Mainz, M. A. J. Siegert, N. A. Jungmann, G. Lesquame, S. Tirat, A. Dreux-Zigha, J. Aszodi, D. Le Beller and R. D. Süßmuth, *Nat. Chem. Biol.*, 2018, **14**, 652–654; (b) S. Chang, Y. Luo, N. He, X. Huang, M. Chen, L. Yuan and Y. Xie, *Front. Chem.*, 2023, **11**, 1233938; (c) J. E. Leet, W. Li, H. A. Ax, J. A. Matson, S. Huang, R. Huang, J. L. Cantone, D. Drexler, R. A. Dalterio and K. S. Lam, *J. Antibiot.*, 2003, **56**, 232–242; (d) A. Mukai, T. Fukai, Y. Hoshino, K. Yazawa, K. I. Harada and Y. Mikami, *J. Antibiot.*, 2009, **62**, 613–619.



- 11 (a) J. Chen, A. Frediansyah, D. Männle, J. Straetener, H. Brötz-Oesterhelt, N. Ziemert, L. Kaysser and H. Gross, *ChemBioChem*, 2020, **21**, 2205–2213; (b) A. Botas, M. Eitel, P. N. Schwarz, A. Buchmann, P. Costales, L. E. Núñez, J. Cortés, F. Morís, M. Krawiec, M. Wolanski, B. Gust, M. Rodriguez, W. N. Fischer, B. Jandeleit, J. Zakrzewska-Czerwińska, W. Wohlleben, E. Stegmann, P. Koch, C. Méndez and H. Gross, *Angew. Chem., Int. Ed.*, 2021, **60**, 13536–13541.
- 12 J. Mistry, S. Chuguransky, L. Williams, M. Qureshi, G. A Salazar, E. L. L. Sonnhammer, S. C. E. Tosatto, L. Paladin, S. Raj, L. J. Richardson, R. D. Finn and A. Bateman, *Nucleic Acids Res.*, 2021, **49**, D412–D419.
- 13 (a) G. Zhong, *ACS Bio Med Chem Au*, 2023, **3**, 371–388; (b) S. Kunakom, H. Otani, D. W. Uduary, D. T. Doering and N. J. Mouncey, *J. Ind. Microbiol. Biotechnol.*, 2023, **50**, kuad005.
- 14 (a) J. D. Rudolf, C. Y. Chang, M. Ma and B. Shen, *Nat. Prod. Rep.*, 2017, **34**, 1141–1172; (b) M. C. Tang, Y. Zou, K. Watanabe, C. T. Walsh and Y. Tang, *Chem. Rev.*, 2017, **117**(8), 5226–5333.
- 15 C. J. Schwalen, G. A. Hudson, B. Kille and D. A. Mitchell, *J. Am. Chem. Soc.*, 2018, **140**, 9494–9501.
- 16 (a) X. Yang and W. A. van der Donk, *Chem.–Eur. J.*, 2013, **19**, 7662–7677; (b) B. J. Burkhart, G. A. Hudson, K. L. Dunbar and D. A. Mitchell, *Nat. Chem. Biol.*, 2015, **11**, 564–570.
- 17 H. Gross, *Appl. Microbiol. Biotechnol.*, 2007, **75**, 267–277.
- 18 T. P. Wyche, A. C. Ruzzini, L. Schwab, C. R. Currie and J. Clardy, *J. Am. Chem. Soc.*, 2017, **139**, 12899–12902.
- 19 R. T. Williamson, A. V. Buevich, G. E. Martin and T. Parella, *J. Org. Chem.*, 2014, **79**, 3887–3894.
- 20 R. J. Juarez, Y. Jiang, M. Tremblay, Q. Shao, A. J. Link and Z. J. Yang, *J. Chem. Inf. Model.*, 2023, **63**, 522–530.
- 21 (a) J. J. Hug, J. Dastbaz, S. Adam, O. Revermann, J. Koehnke, D. Krug and R. Müller, *ACS Chem. Biol.*, 2020, **15**, 2221–2231; (b) P. Nanudorn, S. Thiengmag, F. Biermann, P. Erkoç, S. D. Dirnberger, T. N. Phan, R. Fürst, R. Ueoka and E. J. N. Helfrich, *Angew. Chem., Int. Ed.*, 2022, **61**, e2022083.
- 22 K. Viehrig, F. Surup, C. Volz, J. Herrmann, A. Abou Fayad, S. Adam, J. Köhnke, D. Trauner and R. Müller, *Angew. Chem., Int. Ed.*, 2017, **56**, 7407.
- 23 (a) M. M. Zdouc, M. M. Alanjary, G. S. Zarazúa, S. I. Maffioli, M. Crüsemann, M. H. Medema, S. Donadio and M. Sosio, *Cell Chem. Biol.*, 2021, **28**, 733–739; (b) J. J. Hug, N. A. Frank, C. Walt, P. Senica, F. Panter and R. Müller, *Molecules*, 2021, **26**, 7483.
- 24 K. E. Shelton and D. A. Mitchell, *Methods Enzymol.*, 2023, **679**, 191–233.
- 25 L. Holm, *Nucleic Acids Res.*, 2022, **50**, W210–W215.
- 26 S. K. Burley, C. Bhikadiya, C. Bi, S. Bittrich, L. Chen, G. V. Crichlow, C. H. Christie, K. Dalenberg, L. D. Costanzo, J. M. Duarte, S. Dutta, Z. Feng, S. Ganesan, D. S. Goodsell, S. Ghosh, R. K. Green, V. Guranović, D. Guzenko, B. P. Hudson, C. L. Lawson, Y. Liang, R. Lowe, H. Namkoong, E. Peisach, I. Persikova, C. Randle, A. Rose, Y. Rose, A. Sali, J. Segura, M. Sekharan, C. Shao, Y. P. Tao, M. Voigt, J. D. Westbrook, J. Y. Young, C. Zardecki and M. Zhuravleva, *Nucleic Acids Res.*, 2021, **49**, D437–D451.
- 27 D. S. Froese, J. Kopec, E. Rembeza, G. A. Bezerra, A. E. Oberholzer, T. Suormala, S. Lutz, R. Chalk, O. Borkowska, M. R. Baumgartner and W. W. Yue, *Nat. Commun.*, 2018, **9**, 2261.
- 28 A. W. Struck, M. L. Thompson, L. S. Wong and J. Micklefield, *ChemBioChem*, 2012, **13**, 2642–2655.
- 29 E. G. Gharakhanian and T. J. Deming, *Chem. Commun.*, 2016, **52**, 5336–5339.
- 30 M. S. Puar, T. M. Chan, V. Hegde, M. Patel, P. Bartner, K. J. Ng, B. N. Pramanik and R. D. MacFarlane, *J. Antibiot.*, 1998, **51**, 221–224.
- 31 M. Matsumoto, Y. Kawamura, Y. Yasuda, T. Tanimoto, K. Matsumoto, T. Yoshida and J. Shoji, *J. Antibiot.*, 1989, **42**, 1465–1469.
- 32 B. S. Yun, T. Hidaka, K. Furihata and H. Seto, *J. Antibiot.*, 1994, **47**, 1541–1545.
- 33 M. J. Helf, A. Jud and J. Piel, *ChemBioChem*, 2017, **18**, 444–450.
- 34 (a) K. Watanabe, K. Hotta, A. P. Praseuth, K. Koketsu, A. Migita, C. N. Boddy, C. C. C. Wang, H. Oguri and H. Oikawa, *Nat. Chem. Biol.*, 2006, **2**, 423–428; (b) A. H. Al-Mestarihi, G. Villamizar, J. Fernandez, O. E. Zolova, F. Lombo and S. Garneau-Tsodikova, *J. Am. Chem. Soc.*, 2014, **136**, 17350–17354.
- 35 T. Huang, Y. Duan, Y. Zou, Z. Deng and S. Lin, *ACS Chem. Biol.*, 2018, **13**, 2387–2391.
- 36 B. Shen, L. Du, C. Sanchez, D. J. Edwards, M. Chen and J. M. Murrell, *J. Nat. Prod.*, 2002, **65**, 422–431.
- 37 (a) C. Liao and F. P. Seebeck, *Angew. Chem., Int. Ed.*, 2019, **58**, 3553–3556; (b) F. Trottmann, J. Franke, I. Richter, K. Ishida, M. Cyrulies, H.-M. Dahse, L. Regestein and C. Hertweck, *Angew. Chem., Int. Ed.*, 2019, **58**, 14129–14133; (c) F. Trottmann, K. Ishida, M. I. Ito, H. Kries, M. Groll and C. Hertweck, *Nat. Chem.*, 2022, **14**, 884–890.
- 38 Z. F. Xia, T. W. Guan, J. S. Ruan, Y. Huang and L. L. Zhang, *Int. J. Syst. Evol. Microbiol.*, 2013, **63**, 2813–2818.
- 39 Y. Zhao, E. Marschall, M. Treisman, A. McKay, L. Padva, M. Crüsemann, D. R. Nelson, D. L. Steer, R. B. Schittenhelm, J. Tailhades and M. J. Cryle, *Angew. Chem., Int. Ed.*, 2022, **61**, e202204957.
- 40 (a) D. Guan, F. Chen, Y. Qiu, B. Jiang, L. Gong, L. Lan and W. Huang, *Angew. Chem., Int. Ed.*, 2019, **131**, 6750–6754; (b) J. Zang, Y. Chen, W. Zhu and S. Lin, *Biochem*, 2019, **59**, 132–138; (c) N. L. Kjærsgaard, T. B. Nielsen and K. V. Gothelf, *ChemBioChem*, 2022, **23**, e202200245.

